Lattice Boltzmann Modeling of Carbon Dioxide Injection through Water-saturated Transversal Porous Strips Subject to a Temperature Gradient

Nurbakyt Marat, B.Eng.

Submitted in fulfillment of the requirements

for the degree of Master of Science

in Mechanical & Aerospace Engineering

School of Engineering and Digital Sciences

Department of Mechanical & Aerospace Engineering

Nazarbayev University

53 Kabanbay Batyr Avenue,

Astana, Kazakhstan, 010000

Supervisor: Dr. Luis R. Rojas-Solórzano, Associate Professor

Co-supervisor: Dr. Konstantinos Kostas, Associate Professor

April 2024

DECLARATION

I hereby, declare that this manuscript, entitled "*Lattice Boltzmann Modeling of Carbon Dioxide Injection through Water-saturated Transversal Porous Strips Subject to a Temperature Gradient*", is the result of my own work except for quotations and citations, which have been duly acknowledged.

I also declare that, to the best of my knowledge and belief, it has not been previously or concurrently submitted, in whole or in part, for any other degree or diploma at Nazarbayev University or any other national or intentional institution.

Name: Nurbakyt Marat

Date: 26.04.2024

Abstract

Carbon dioxide (CO_2) sequestration in underground aquifers offers a viable solution to mitigating global warming by reducing atmospheric greenhouse gas concentrations. However, the efficiency of this process depends on intricate heat transfer dynamics, necessitating comprehensive numerical and experimental analyses. Conventional computational fluid dynamics (CFD) methods and experimental approaches often fail to capture the complexities of CO_2 sequestration. Unlike previous studies, which primarily focused on homogeneous porous layers, this study employs the mesoscopic Lattice Boltzmann Method (LBM) to investigate fluid displacement and heat transfer in the CO_2 injection through spanwise porous layers of varying porosities initially saturated with water and sandwiched between parallel heating plates. The investigation of the dynamics of CO_2 injection offers a novel perspective on fluid displacement, addressing the influence of the Richardson number, a key indicator of the balance between natural and forced convection. The ultimate objective of this study is to identify the most efficient regime for transporting fluids, specifically CO_2, through these heterogeneous porous layers. Multiple Richardson numbers are examined to comprehensively understand the roles of natural and forced convection. The results are analyzed and correlated with the average Nusselt number, providing valuable insights into optimizing fluid transport within porous structures. This research advances the understanding of CO_2 sequestration and contributes essential knowledge for developing efficient and cost-effective strategies in combating climate change through underground carbon dioxide storage.

Table of Contents

List of Abbreviations & Symbols

CFD	Computational Fluid Dynamics
LBM	Lattice Boltzmann Method
T	Temperature
lu	Lattice unit
ts	Time step
h	Height
θ_1	Contact angle
w	Width
BC	Boundary conditions
RB	Rayleigh-Benard
Ra	Rayleigh number
Nu	Nusselt number
T_s	Surface temperature
T_f	Fluid temperature
Gr	Grashof number
Re	Reynolds number
Ri	Richardson number
Kn	Knudsen number

Chapter 1 – Introduction

1.1. Background

Carbon dioxide is the main contributor to the rise of greenhouse gas emissions, as CO_2 emissions rose to 36.3 Gigatons by the end of 2021, being the highest level of CO_2 emissions in history, according to the International Energy Agency [1]. Carbon dioxide sequestration is the process of carbon capture and storage (CCS), one of the leading solutions for reducing greenhouse gas emission concentration in the atmosphere [1], [2]. Figure 1 shows the scheme of CCS, which depicts three main stages: CO_2 capturing from the plants, CO_2 transportation through pipes, CO_2 injection into the well, and storage underground by displacing water [2].

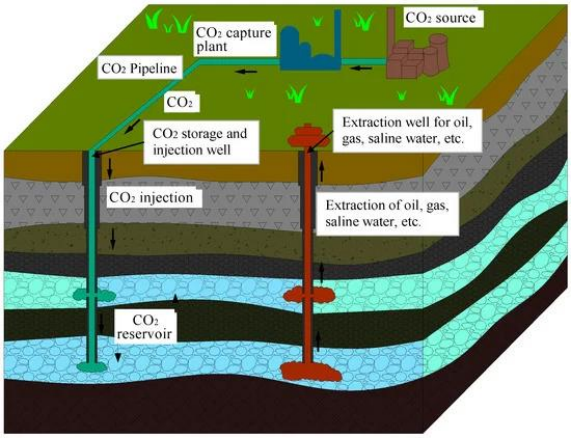

Figure 1. Carbon capture and storage [2].

However, CO_2 sequestration is still expensive and complex to conduct experimental investigations and implement in the industry; hence, numerical studies are needed [3], [4]. This problem can be solved by using a numerical approach such as the "Lattice Boltzmann Method (LBM)," which is more computationally efficient than traditional Computational Fluid Dynamics (CFD) [5]-[7].

This work investigates the parameters and conditions surrounding the heat transfer mechanisms occurring during CO_2 sequestration in the layers of a porous medium. CO_2 sequestration is a complex problem that includes the convection-diffusion-dissolution process, including thermal and chemical reactions. Nevertheless, the process has been previously studied

mainly as a displacement under isothermal conditions, ignoring thermal phenomena such as convection [4]. The thermal Lattice Boltzmann Method on mesoscale will help solve this challenge. Based on the Boltzmann equation, the mesoscopic approach simulates the fluid as a discrete particle set. The LBM uses a lattice to represent the space, dividing the fluid into discrete cells [6]. There are two main advantages of LBM. First is a mesoscopic method, i.e., a combination of macro and microscales. Secondly, LBM can handle arbitrary complex geometries and boundary conditions, and it is well-suited for parallelizing, so the computing time decreases compared to standard CFD solutions [5] – [7].

This study employs the Lattice Boltzmann Method (LBM) to investigate fluid displacement and heat transfer during CO_2 injection through spanwise porous layers with varying porosities. Initially saturated with water, these layers are situated between parallel heating plates. The research focuses on understanding the impact of the Richardson number, a crucial parameter indicating the balance between natural and forced convection. In contrast to prior studies that concentrated on homogeneous porous layers, this research explores the dynamics of CO_2 injection through alternating porous layers, offering a new perspective on fluid displacement. The primary goal is identifying the most efficient regime for transporting fluids, specifically CO_2, through these heterogeneous porous layers. Multiple Richardson numbers are considered to understand the roles of natural and forced convection comprehensively. The results are meticulously analyzed and correlated with the average Nusselt number, providing valuable insights for optimizing fluid transport within porous structures.

1.2. Motivation

This research contributes to advancing the understanding of CO_2 sequestration and provides essential knowledge for developing efficient and cost-effective strategies to combat climate change through underground carbon dioxide storage. The primary benefit will be creating new knowledge to support global sustainability and positioning Kazakhstan as a responsible and compliant country with a fossil fuel-based economy.

1.3. Research Objectives

The primary aim is to explore the heat transfer process in the context of carbon dioxide sequestration within vertically layered porous media. Objectives:

1) Investigating the displacement of CO_2 under the conditions of two distinct vertical porous strips with varying Richardson numbers.
2) Establishing a connection between the Richardson and Nusselt numbers during CO_2 sequestration.

Chapter 2 – Literature Review

2.1. Lattice Boltzmann Method

The lattice Boltzmann method (LBM) is a computational fluid dynamics (CFD) technique that models single and multiphase fluid flow behavior. Based on the Boltzmann equation, the mesoscopic approach simulates the fluid as a discrete particle set. The LBM tool uses a lattice to represent the space, dividing the fluid into discrete cells [6]. There are two main advantages of LBM. First is a mesoscopic method, a combination of macro and microscales. Secondly, LBM can handle arbitrary complex geometries and boundary conditions, and it is well-suited for parallelizing, so the computing time decreases compared to standard CFD solutions [5] – [7].

Researchers are investigating heat transfer applications to different LBM approaches [11] – [22]. The base of LBM relies on the distribution function for velocity and temperature field [6]. Heat transfer is described separately in fluid dynamics [9]. The joint of LBM and heat transfer makes modeling possible to have an appropriate physics in the domain [10].

Lattice Boltzmann Method (LBM) can also be an alternative to conventional numerical methods such as Finite Volume Method (FVM). In reference [37], the results obtained using LBM and FVM for a heat transfer problem in a porous medium were compared. The findings revealed consistency between the two methods, specifically in terms of temperature propagation and radiative heat flux along the length of the cavity.

2.2. Heat Transfer in the porous medium

2.2.1. Utilizing different numerical methods

Heat transfer of fluid flows in porous media mainly studies convection in three primary length scales: pore-scale (cannot give realistic engineering solutions due to its limited nature), region/domain scale (offers only a broad range of information for the whole reservoir, computationally inefficient limiting to show the specific areas of interest); representative element volume (REV) (balanced scale within pores and domains and most popular among all three) [10].

Thermal convection is a widespread occurrence in both natural phenomena and technological applications. Rayleigh-Bénard (RB) convection, characterized by fluid movement

in a container heated from below and cooled above, is a paradigm for examining thermal convection. This phenomenon has undergone comprehensive study over the past few decades [35].

In reference [38], the study focuses on analyzing the performances of the Genetic Algorithm (GA) and the Global Search Algorithm (GSA) in simultaneously estimating properties during heat transfer in the porous matrix. They discovered that convective heat exchange between the gas (air) and the solid porous matrix is influenced by the airflow at a constant velocity.

2.2.2. Utilizing LBM

The REV-scale porous medium is like a continuum (geometries in details are ignored), and thus, to model the presence of the porous structure in the flow path, additional sub-modeling is needed, i.e., the Darcy flow equation and Brinkman-extended-Darcy flow equation [9], [10] are coupled into the LBM. Porosity, permeability, and thermal conductivity are included in the LB equations. REV-scale method accuracy is dependent on the semi-empirical models, but they are not applicable when the porosity of the domain changes [21]. Nevertheless, the REV scale is more computationally efficient than the mesoscale modeling and can produce valuable outcomes of a larger-scale porous system. However, this model is applicable for homogeneous porous medium [9].

In recent decades, heat transfer simulations utilizing LBM [8, 11, 12], particularly in the porous cavity, have been developed significantly [9], [13] – [25]. The heat transfer numerical modeling of natural convection in a square domain without porous medium using least square LBM and Taylor Series expansion began in 2002 [11]. D'Orazio et al. [12] proposed a thermal lattice BGK (Bhatnagar-Gross-Krook) model called collision operator with a single relaxation time that selects the equilibrium distribution function to restore the incompressible Navier-Stokes equations at low Mach numbers. The proposed model boundaries are non-thermal top and bottom, high- and low-temperature incorporated vertical wall boundary conditions in a 2D square domain. A recent study in 2019 [8] introduced inclined cavities to optimize natural convection. It justified that inclination at 30 degrees could increase heat transfer from hot to cold wall vertical walls in single-phase – supercritical carbon dioxide.

Fluid Flow in the porous medium was the subject of interest to numerous researchers due to its complexity and instability [10]. One of the primary fluid parameters - viscosity can affect the heat transfer rate [13]. Researchers of flows with temperature-dependent viscosity [13]

incorporated the Darcy effect, mentioning the Darcy parameter's importance in the modeling [9], [11], [12], [18]. Even though authors [13] ignored the heterogeneous nature of realistic porous media, one year later, in 2006, Yan et al. [14] introduced heat transfer in a heterogeneous porous medium. They found out that porosity in the center of a cavity has little effect on heat transfer. Heat transfer is stimulated mainly by the pores of the near-wall zone [14].

Zhao et al. [15] incorporated a porous medium into the thermal BGK with the doubled populations method proposed in [12]. They concluded that heat transfer could speed up with a pore density increase but slow with the increase in porosity. Ouakad [16] studied the classic problem of Rayleigh-Benard convection by various Rayleigh numbers (Ra) and showed that low values of Ra lead to a steady state. In contrast, high Ra causes instability and viscous fingering. Researchers [16] assumed the dissolution of carbon dioxide in the brine and ignored turbulence, which resulted in the Rayleigh-Benard type of convection that occurs in the domain without porosity. In contrast, a porosity of 90% results in a steady temperature contour [16], even though another research [20] highlighted the importance of including turbulence and choosing careful parameters to prevent non-physical outcomes.

The Lattice Boltzmann equation can be diverse with the application of different models. Previous work [18] incorporated the effect of porous media into the Cascaded Lattice Boltzmann Method (CLB) in the REV scale. Chen et al. [19] revealed the impact of the Prandtl (Pr), Rayleigh (Ra), and Darcy (Da) numbers in the 3D simulation. Variation of Nusselt number varies in the specific zones for Prandtl number, but a high Prandtl number leads to instability; an increase in porosity, Darcy, and Rayleigh number will lead to an increase in Nusselt number. However, this dependence could not be detected in the small Prandtl number values [19]. Table 1 below represents improvements made by researchers in the heat transfer simulations by LBM.

The Literature Review summarized in Table 1 shows that heat transfer between two immiscible fluids in the heterogeneous porous medium needs to be carefully studied, especially water displacement by supercritical CO_2. Consequently, this work focuses on the heat transfer simulations from supercritical CO_2 to displace water in the multilayered porous medium.

Table 1: Development in the field of heat transfer LBM

References	Year of publication	Novelty/Method	Findings	Advantages	Limitations
[13]	2005	Using temperature-dependent viscosity in a homogenous porous medium.	Viscosity variations increase the Nusselt number compared to constant viscosity; thus, heat transfer also rises.	Importance of viscosity is shown.	Only one phase is present: homogeneous porous medium, which is not applicable in real-life physics.
[14]	2006	2D natural convection in a heterogeneous porous medium.	Porosity in the center of the cavity has less effect on heat transfer than the near-wall zone.	Heterogeneous porous medium is included.	One phase
[15]	2010	Development of thermal BGK with doubled populations in the porous medium.	High porosity reduces heat transfer, but pore density is proportional to heat transfer.	Porosity variations effect is included	One phase
[16]	2013	Assuming miscible fluid displacement and porosity	High Rayleigh number causes instability; low Rayleigh number causes Rayleigh-Benard convection type.	Classic problem with porosity and miscible fluid simulation is studied.	Miscible displacement. Lack of porosity variations.
[22]	2017	Non-orthogonal MRT-LBM in a porous cavity with DDF and Hybrid approach.	Non-orthogonal MRT-LBM method shows more stability than BGK-LBM.	New approach: clear numerical definition.	Mixed flow convection.
[19]	2021	3D LBM for large Prandtl number.	High Prandtl number leads to instability; an Increase in porosity, Darcy, and Rayleigh numbers will lead to an increase in the Nusselt number.	Apparent effect of Ra, Da, and Pr numbers is shown.	One phase, homogeneous porous medium.

2.3. Layered porous layers

2.3.1. Using different numerical methods

Numerous variations of the fundamental problem have been explored to examine the impact of additional physical phenomena on convection [26]. Many naturally existing substances exhibit some level of heterogeneity and anisotropy. Several studies have delved into understanding how heterogeneity or anisotropy influences the development of convection from a distributed source [26-28]. Although heterogeneity and anisotropy can vary widely, certain common forms, such as layering, are frequently observed in natural media. A prior numerical investigation conducted in reference [28] focused on examining the influence of a thin layer, highlighting various qualitative aspects of how the layer impacted convective flow. However, this study did not proceed to explore the problem theoretically or provide quantitative scaling to characterize different behaviors.

A related experimental study [32] utilized a horizontal line of posts positioned across a Hele-Shaw cell to create a narrow region with higher resistance to flow. Interestingly, this model did not constitute a macroscopic low-permeability layer. Instead, the flow across the region was primarily influenced by the local geometry of the posts and the gaps between them, which were comparable in scale to the downwelling convective fingers, including dissolution.

In a broader context, the influence of layered heterogeneity on convection has been investigated in various scenarios. Experimental and theoretical studies have focused on the behavior of isolated plumes within layered media, particularly concerning a step jump in permeability [29, 30]. Numerical and theoretical analyses have also been conducted to understand the dynamics of an isolated plume crossing a single thin, low-permeability layer [31].

One of the recent works conducted by D.R.Hewitt [31, 33], published in Cambridge University Press, was related to a convection study in thin, low-permeable horizontal layers using the finite-difference method. The layers can be characterized by their impedance, represented by Ω, a dimensionless ratio of the effective layer thickness to permeability. Meanwhile, the strength of convection is governed by the dimensionless distance, H, between layers—a parameter that can be interpreted as an effective Rayleigh number for the flow. In cases of sufficiently low impedance,

the layers have a negligible effect on the flow. Conversely, higher impedance levels cause the layers to act as a buffer, reducing the strength of convection [33].

Examining convection issues in layered porous media primarily involved employing impedance models or modifying equations to represent permeability and applying horizontal layers using techniques such as the finite-difference method. Works mainly emphasized mass transfer, not encompassing heat transfer.

In this field of investigation, only one paper analyzed heat transfer in the vertical layered porous medium. In reference [36], researchers examined the thermo-diffusion effects on heat and mass transfer in a system consisting of two vertical porous layers heated from one side with varying permeability. The model schematic is shown in Figure 2. The observation is that the impact of heterogeneity on heat transfer intensifies with an increase in the Soret number and a decrease in the Dufour number.

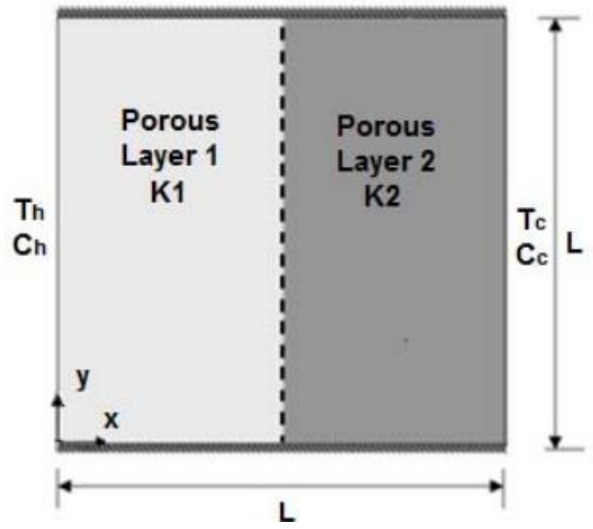

Figure 2. Schematic model of layered porous medium [36] (T_h – hot temperature, T_c – cold temperature, K1 and K2 are permeabilities of two layers).

2.3.2. Using LBM

In the field of LBM, there are few investigations related to porous layers. In reference [34], the enclosure was filled with two parallel horizontal porous layers characterized by distinct porosities. Simulations, accounting for the impact of temperature-dependent viscosity, were conducted using the Lattice Boltzmann method (LBM) at the representative elementary volume

(REV) scale. They found that a higher porosity corresponds to improved heat and mass transfer enhancement as the buoyancy ratio increases. Nevertheless, they did not analyze the heat transfer within the region between the two layers.

Chapter 3 – Methodology

3.1. Lattice Boltzmann equation for the Velocity Field

In multiphase flow simulations, modeling interfaces using conventional Computational Fluid Dynamics (CFD) methods can be computationally expensive. The computational cost notably increases when a solid sub-domain phase is incorporated into a porous structure. In the Lattice Boltzmann Method (LBM), on the other hand, the interface between the solid and multiphase fluid phases is preserved, and complex geometries are seamlessly integrated into the grid. This characteristic of LBM reduces computational costs for handling complex interfaces and porous structures.

In the LBM, the fluid is presented by a set of distribution functions describing the probability of discrete particle collision at a particular point in the lattice with a known velocity. The distribution functions evolve and are updated using collision rules [6]. Figure 3 illustrates a 2D model with nine velocity directions of a particle (D2Q9) used in the simulations.

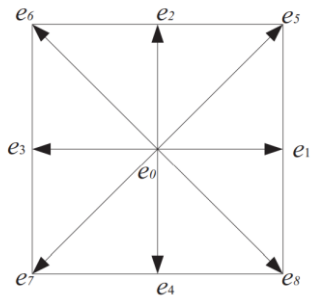

Figure 3. The D2Q9 lattice velocity model [8]

The LBM equation proceeds from the kinetic equation. It computes macroscopic parameters from the probability distribution function $f_i(\vec{x}, t)$, where $\vec{x}$ is position, $\vec{c}_i$ particle velocity, and t time step.

$$f_i(\vec{x} + \vec{c}_i \Delta t, t + \Delta t) = f_i(\vec{x}, t) + \Omega_i(\vec{x}, t) \quad (1)$$

In Eq. (1), the Left-Hand Side (LHS) represents the streaming term, responsible for calculating the advancement of the model between timesteps. The Right-Hand Side (RHS) corresponds to the collision step derived from the Boltzmann equation, which originates from the

kinetic theory of gases. $\Omega_i(\vec{x},t)$ is the collision operator showing particle interaction; in this research, Bhatnagar-Gross-Krook (BGK) operator will be used [23].

$$\Omega_i(f) = \frac{f_i - f_i^{eq}}{\tau}\Delta t \tag{2}$$

Where τ is the relaxation time of the probability distribution function toward the equilibrium function f_i^{eq}.

The equilibrium distribution is derived from Maxwell-Boltzmann equilibrium by:

$$f_i^{eq}(\vec{x},t) = w_i\rho\left(1 + \frac{\vec{u}\cdot\vec{c}_i}{c_s^2} + \frac{(\vec{u}\cdot\vec{c}_i)^2}{2c_s^4} - \frac{\vec{u}\cdot\vec{u}_i}{2c_s^2}\right) \tag{3}$$

Where ρ is density, $\vec{u}$ is macroscopic velocity, w_i are weights factors, c_s and is the speed of sound. Equation (9) outlines the connection between relaxation time τ and kinematic viscosity ν [9].

$$\nu = c_s^2\left(\tau - \frac{\Delta t}{2}\right) \tag{4}$$

Propagation is the left-hand side, and collision is the right-hand side of equations (5) and (6).

$$f_i^*(\vec{x},t) = f_i(\vec{x},t) - \frac{\Delta t}{\tau}\left(f_i(\vec{x},t) - f_i^{eq}(\vec{x},t)\right) \tag{5}$$

$$f_i(\vec{x} + \vec{c}_i\Delta t, t + \Delta t) = f_i^*(\vec{x},t) \tag{6}$$

The Lattice Boltzmann method employs dimensionless quantities for computations, denoted in terms of Lattice Units (LU). Macroscopic density $\rho(\vec{x},t)$ and momentum $\rho\vec{u}(\vec{x},t)$ can be found from discrete particle functions (7) and (8), respectively:

$$\rho(\vec{x},t) = \sum_i f_i(\vec{x},t) \tag{7}$$

$$\rho\vec{u}(\vec{x},t) = \sum_i \vec{c}_i f_i(\vec{x}t) \tag{8}$$

3.2. Lattice Boltzmann equation for the Temperature field

Similarly to its application in multiple fluid systems, the Lattice Boltzmann Equation (LBE) method can be extended to address problems involving diffusion and heat transfer. This extension incorporates additional distribution functions for each solute and temperature, allowing the LBE method to effectively model the relevant transport phenomena in diverse scenarios [40, 41].

Heat transfer through conduction is modeled using the following equation for h_i - heat distribution function:

$$h_i(\vec{x} + \vec{e_i}\Delta t, t + \Delta t) - h_i(\vec{x}, t) = -\frac{\Delta t}{\tau_t}[h_i(\vec{x}, t) - h_i^{eq}(\vec{x}, t)] \quad (9)$$

where τ_t is thermal relaxation time and $h_i{}^{eq}$ is equilibrium distribution function. The following equation is used to calculate equilibrium:

$$h_i^{eq}(\vec{x}, t) = w_i T\left(1 + 3\frac{\vec{u}.\vec{e_i}}{c_s^2}\right) \quad (10)$$

where the temperature of lattice point T is calculated as a sum of heat distribution functions in every direction,

$$\mathrm{T}(\vec{x}, t) = \sum_i h_i(\vec{x},\ t) \quad (11)$$

and thermal diffusivity α is calculated from thermal relaxation time,

$$\alpha = \frac{1}{3}(\tau_t - \frac{1}{2}) \quad (12)$$

The effect of buoyancy is modeled using the Boussinesq approximation [42], which is applied as an additional force like:

$$\vec{F}_{bous} = -\rho\vec{g}\beta(\frac{T - T_0}{T_h - T_l}) \quad (13)$$

where $\vec{g}$ is gravity vector β is the thermal expansion coefficient, T_h and T_l are the highest and the lowest temperatures in the model, respectively, T_0 is the medium temperature between T_h and T_l.

For quantitative analysis of the results, Grashof (Gr) and Reynolds (Re) numbers are used, shown in eq.14 and 15:

$$\mathrm{Gr} = \frac{g\beta(T_s - T_\infty)D^3}{\nu^2} \quad (14)$$

$$\mathrm{Re} = \frac{uL}{\nu} \quad (15)$$

where T_s and T_∞ are temperatures on the surface and bulk, respectively, and D and L are characteristic lengths perpendicular and parallel to the inlet flow direction, respectively.

To quantify the ratio of buoyancy to inertial forces, i.e., natural to forced convection, Gr over Re squared, also denoted as Richardson number (Ri), is used [43]. The Grashof number's ratio to the Reynolds number's square can be used to assess if forced or free convection in a system can be ignored or if the two coexist. It is possible to ignore free convection if this ratio is significantly smaller than one. It is possible to ignore forced convection if the ratio is considerably larger than one. Otherwise, forced and free convection are combined in the mode [43].

$$Ri > 1 \rightarrow natural\ convection$$
$$Ri < 1 \rightarrow forced\ convection$$
$$Ri \approx 1 \rightarrow mixed\ convection$$

3.3. Nusselt number

Nusselt number calculation indicates the convective to conductive heat transfer ratio at a boundary fluid as a dimensionless value. The general formulation of the Nusselt number (Nu) is as follows:

$$Nu = \frac{hL}{k} \tag{16}$$

Where h is the convective heat transfer coefficient, L is the characteristic length of the flow, and k is the fluid's thermal conductivity.

General forms heat rates due to convection and conduction were implied for the mathematical formulation of the Nusselt number, as in the model, the heat transfer coefficient and conductivity of the fluid are unknown. The multiphase nature of simulations raised the need to use the first-order finite difference method. Heat rate due to convection:

$$\dot{Q}_{conv} = hA\left(T_s - T_f\right) \tag{17}$$

Where T_s and T_f are the surface and fluid temperatures, and A is the area.

Heat rate due to conduction:

$$\dot{Q}_{cond} = -kA\frac{\partial T}{\partial y}\Big|_{at\ y=0} \tag{18}$$

Calculations of the average Nusselt number were done according to [44]. Lines between obstacle columns are plotted to extract temperature values. Each line represents a value of the Nusselt number at x, while the average value represents one layer.

Nusselt number at x (Eq.19) and average Nusselt number (Eq.20):

$$Nu_x = \frac{\partial T^*}{\partial y^*}\Big|_{y^*=0} \tag{19}$$

$$\overline{Nu} = \frac{\int Nu_x dx}{D^*} \tag{20}$$

Where * is dimesionless measure, D^* corresponds to the dimensionless x-length of the one layer.

Chapter 4 – Model set-up

The model domain was set as 601x301(Fig.4). The Domain was chosen due to mesh convergence in the previously presented reference [39]. In physical units, the channel length is 1.4 x 10^{-6} m, and the channel width is 7.1 x 10^{-7} m. Multiphase fluid simulations were undertaken through two transversal porous strips with the following BC:

- Inlet (CO_2 is injected from the left) with a fixed velocity of 0.004 lu/lattice time (in physical units, it is 10.26 m/s);
- Outlet.
- Top wall: cold with a temperature of 0 lattice units.
- Bottom wall: heated uniformly at a temperature of 1 lattice units.

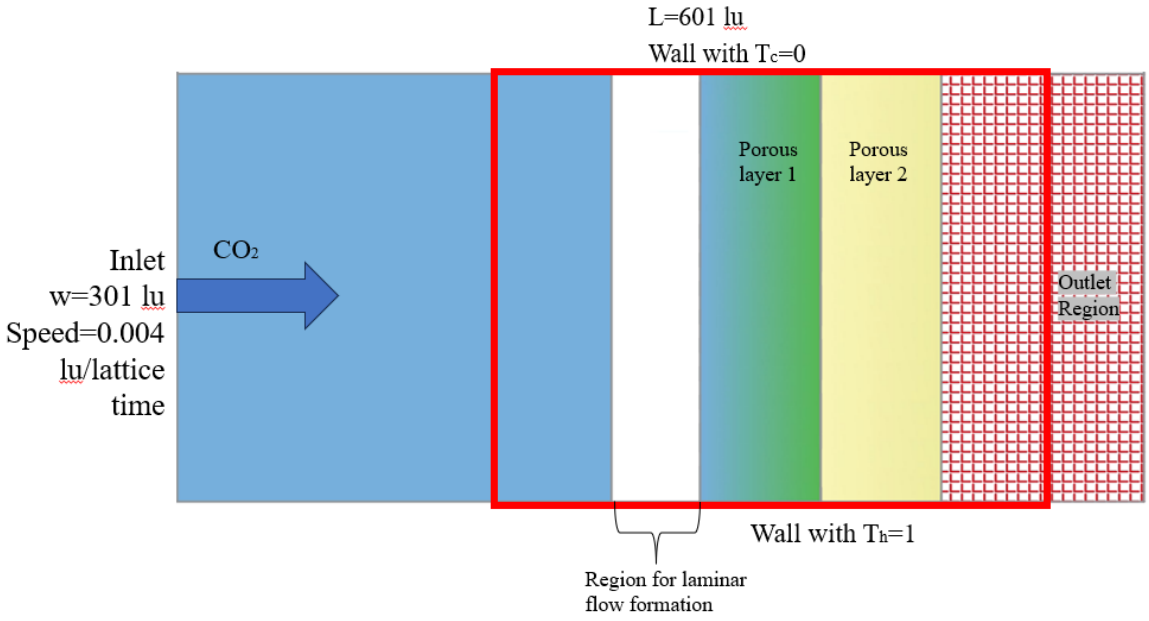

Figure 4. Model setup.

The red rectangle indicates the zone of interest. The porous layers were selected with 29, 44, and 66% porosity. The combination of the layers is shown in Table 2:

Table 2: Layer porosities

Layer 1, %	Layer 2, %
66	41
66	29
41	66

41	29
29	66
29	41

Chapter 5 – Validation of the model

5.1. Immiscibility test

Figure 5 depicts a conducted validation, wherein a stationary H_2O droplet with a diameter of 30 lattice units (LU) is positioned at the center of a square domain filled with CO_2 after 10,000 timesteps. The domain size is 201×201 lattice units (LU^2), with solid boundaries on all four sides. The chosen interaction parameter for this simulation is g=2.5, selected for its stability.

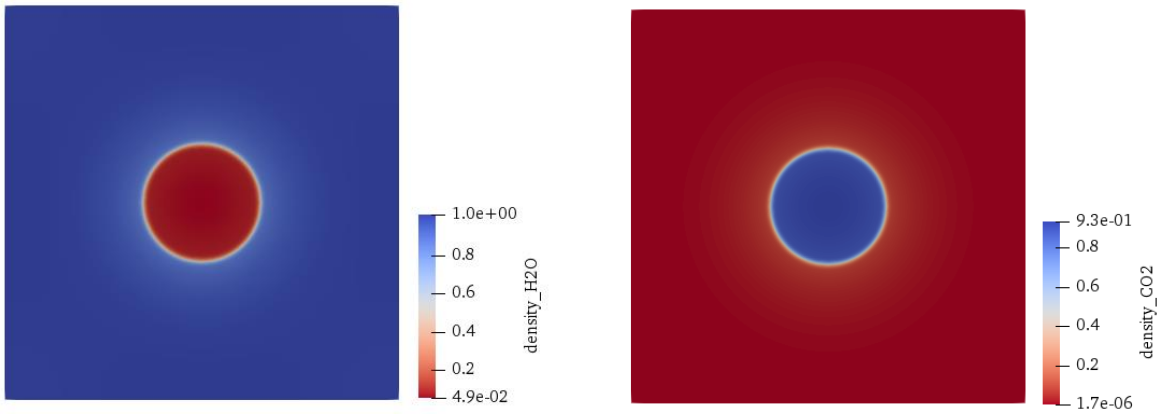

a) Density of H_2O (blue) b) Density of CO_2 (red)

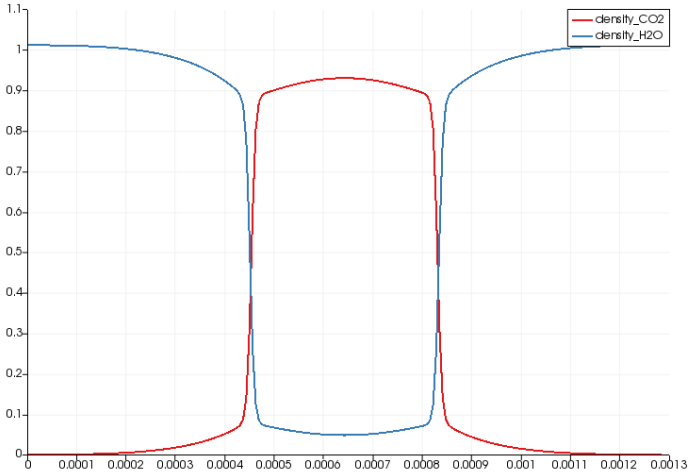

c) Density profile (in LU) taken at the vertical centerline of the cross-section of the domain

Figure 5. A static CO_2 droplet is in equilibrium within an H_2O-saturated medium.

5.2. Rayleigh-Benard convection problem in a rectangular cavity

To validate the thermal model, Rayleigh-Benard (RB) one-phase in a rectangle cavity was simulated, and the results were compared to references [48], [49], and [50]. All fluid attributes were set to zero, and the boundary conditions were the same. The bottom wall was intended to be hot, while the top wall was set to be cold. The average Nusselt numbers were compared near the hot wall by varying the Rayleigh number (see Table 3).

Table 3: Comparison of average Nusselt number near the hot wall

Rayleigh number	$5x10^3$	10^4	$5x10^4$
[48]	2.116	2.661	4.245
[49]	2.104	2.644	4.133
[50]	2.121	2.655	4.191
Present work	2.135	2.667	4.126

As shown in Table 3, the findings in each example are very similar to those in the literature, and these comparisons support the numerical approach used, which may yield accurate results. Figure 6 depicts streamlines for the single-phase RB issue with Ra = 10^4.

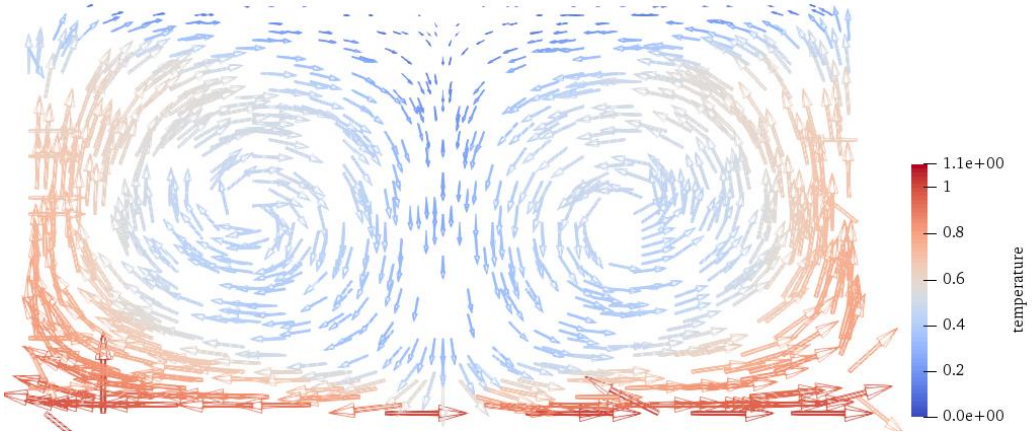

Figure 6. Streamlines of one-phase RB convection.

5.3. Knudsen number

In fluid mechanics and gas dynamics, the Knudsen number is a dimensionless parameter used to describe gas flow in porous media. It allows us to determine the limits of the continuum assumption when considering CO_2 transit via the porous medium. The Knudsen number is defined as:

$$Kn = \frac{\lambda}{L} \tag{21}$$

Where λ is the molecule's mean free path, and L is the characteristic length.

The Knudsen number is instrumental when determining the boundary conditions on walls in fluid flows. Typically, the flow at a flow field's boundary, where the channel walls are fixed in space, is assumed to be stationary, and the liquid in direct contact does not move. The no-slip boundary condition states no relative movement (slip) between the wall and the fluid and applies when the fluidic system's characteristic length exceeds the mean free path.

Typically, the anticipated threshold value is Kn < 0.001. Suppose the fluid system's characteristic dimension is reduced to a value approaching the mean free path. In that case, the fluid molecules near the wall will have a substantial average movement relative to the wall. The Knudsen number has a distinctive range of 0.001 to 0.1. In this scenario, the slip boundary condition is assumed. There is no validity for the continuum assumption for Knudsen values greater than 0.1, and the fluid flow dynamics must be defined statistically. Because liquids are incompressible, the mean free path may be considered constant [46].

In our analysis, the Knudsen number (Kn) is the ratio of the mean free path of a CO_2 molecule in critical conditions to the pore length in the model. Typical aquifer conditions for CO_2 sequestration frequently have a low Knudsen number due to high pressures and temperatures, resulting in flow behavior that follows the continuum assumption. The mean free path of the CO_2 is 1.18 nm in critical conditions, which is the distance that a CO_2 molecule travels before collision with other molecules. In our analysis, the pore's characteristic size corresponds to the pore's length in the porous medium, 0.176 mm. Thus, in our model, the Knudsen number is **0.0067**, which supports the assumption of the fluid as a continuum. According to [47], LBM can be applied to

the full continuum and even to slip conditions when the Knudsen number is between 0.001 and 0.1.

5.2. Sensitive analysis

Sensitivity analysis is vital for validating and analyzing complicated simulation models [51]. The current investigation aims to assess the individual influence of porosity variation on the CO_2 transport time. It is the theoretical time it takes to transport the CO_2 into the porous medium, as porosity is one of the essential factors affecting the sensitivity time [52] under a given pressure gradient. This analysis considers the time required to transport the CO_2 from the inlet to the end of the second layer of the porous medium. The sensitivity time varies according to porous layer construction and justifies the consideration of Nu_x and $\overline{Nu}$ at different timesteps in different cases. The sensitivity time is found as follows:

$$Sensitivity\ time = \frac{distance}{velocity} = \frac{\varphi_1 L_1}{v} + \frac{\varphi_2 L_2}{v} \tag{22}$$

Where φ_1 and φ_2 are the porosities of layers 1 and 2, respectively, L_1 and L_2 are the layer thicknesses, and v is the velocity.

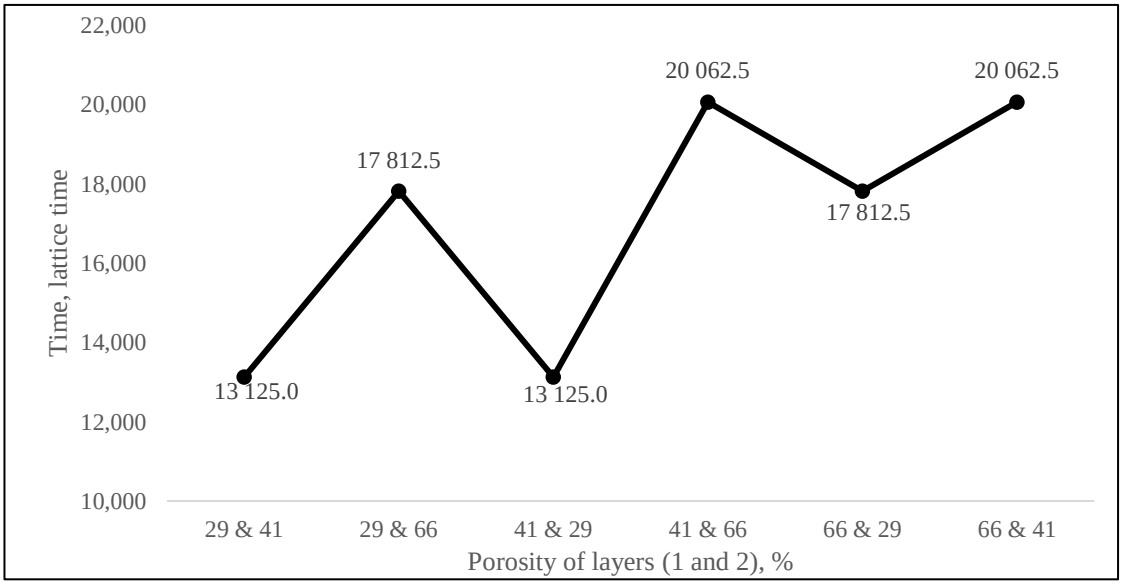

Figure 7. Sensitivity time in ts(lattice time) for each case.

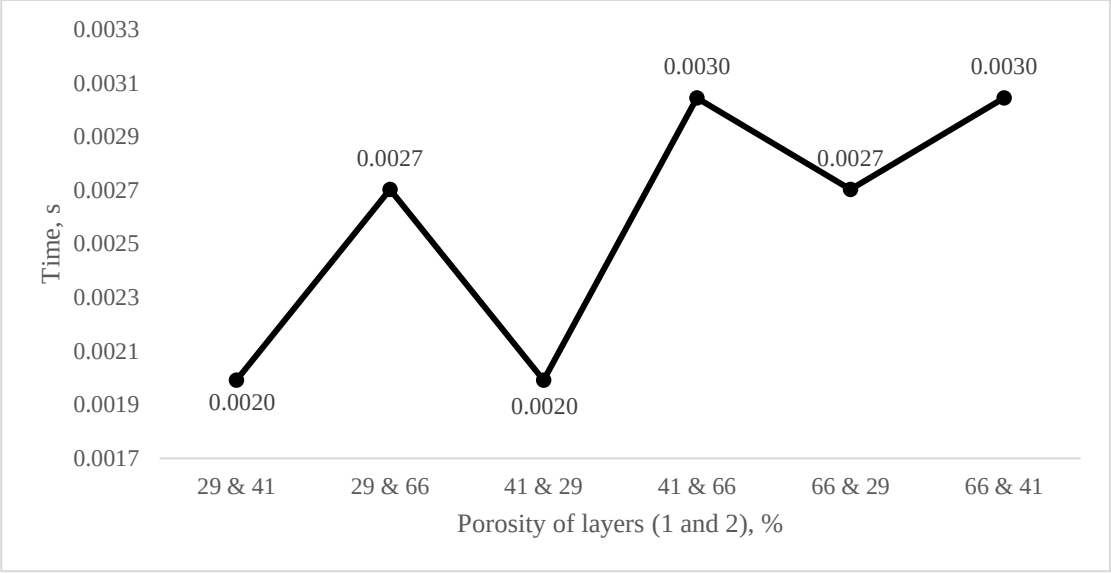

Figure 8. Sensitivity time in seconds for each case.

Figures 7 and 8 show the timesteps and seconds when CO_2 reaches the outlet region by crossing the second layer of the porous medium. The highest time for CO_2 to reach the outlet is found for the 41% and 66% porosities. The shortest time for CO_2 to reach the end of the second layer is found for 29% and 41% porosities. Therefore, the time for CO_2 to travel through the porous medium varies with the porosity combination; consequently, for our simulations, different time steps should be applied to reach a similar condition in all cases and then to calculate the respective Nusselt number. However, this is an approximation, judged sufficient in our case, to predict that sensitive time, given that the fluid is intrinsically compressible and the exact time values may vary slightly.

Chapter 6 – Results

6.1. Nusselt number at x-position

The Nusselt number at an x-position was calculated by plotting additional (yellow) lines in the model, as shown in Fig. 9.

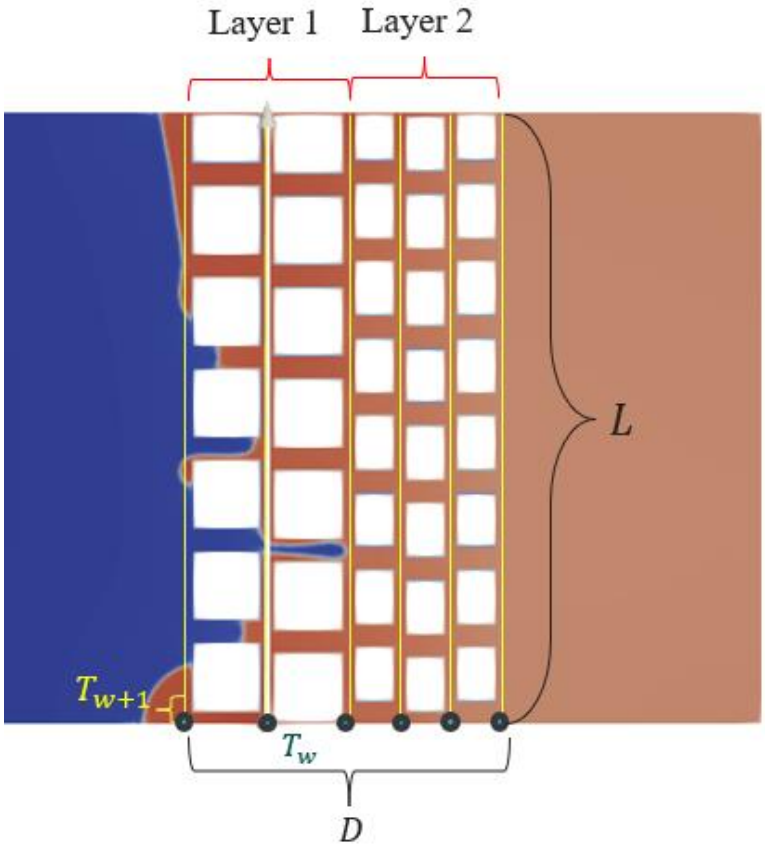

Figure 9. Schematic diagram of line plotting for Nusselt number calculation.

Figures 10 and 11 illustrate the Nusselt number corresponding to 0.01, 1, and 2 Richardson numbers. The Nusselt number trend at the x-position remains consistent across all three Richardson number values. Variations in porosity impact the quantified values, demonstrating that convective heat transfer predominates in different Richardson number scenarios. In most cases, the Nusselt number exceeds 10, indicating the dominance of convective heat transfer.

Porosity of the layer 1 & 2	Ri=0.01	Ri=1	Ri=2

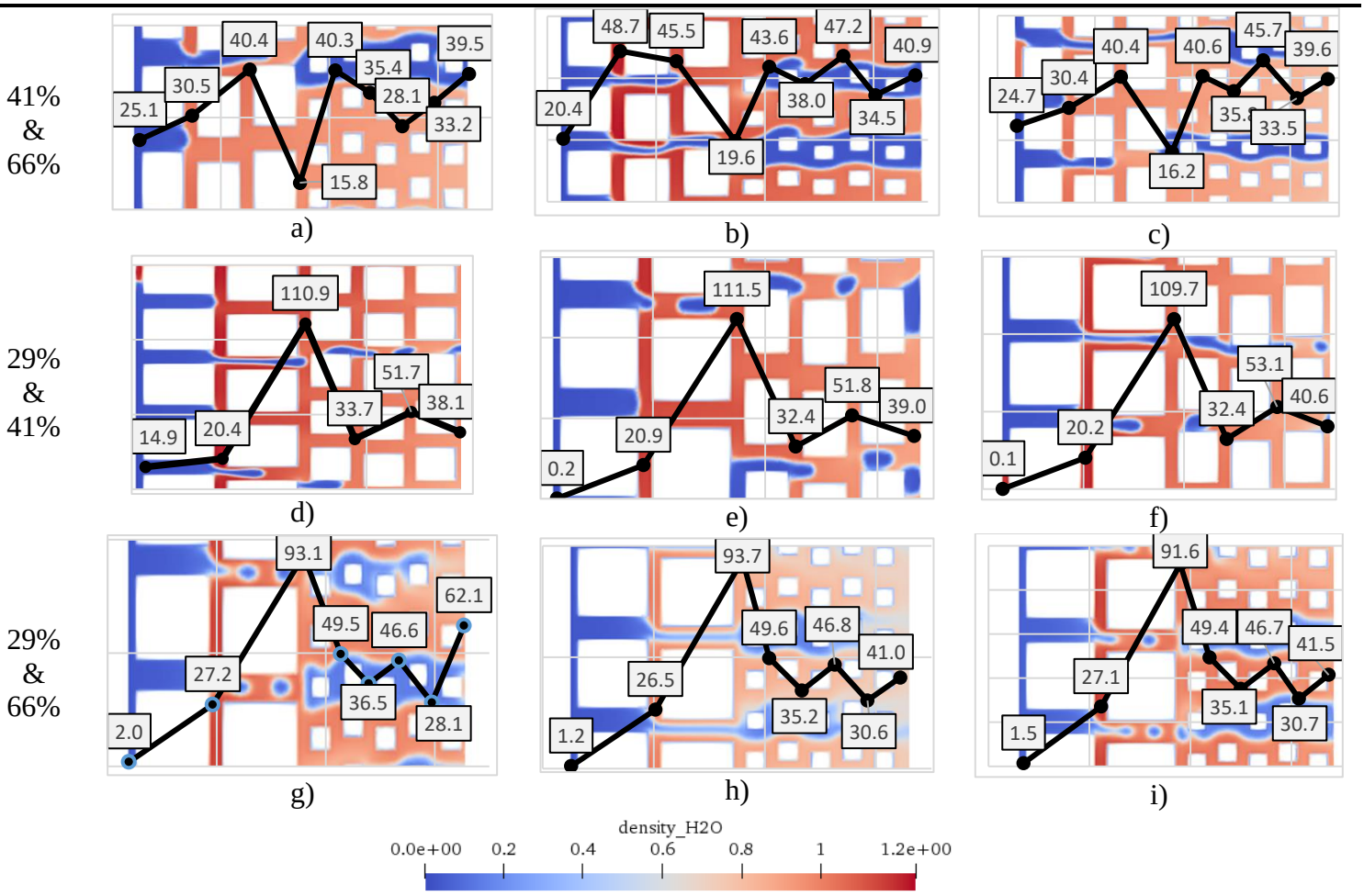

Figure 10. Nusselt number at x-position in the cases of increasing porosity

Figure 10 depicts scenarios involving different porosity levels in two layers. When the first layer has a lower porosity and the second layer has a higher porosity (Fig. 10a, 10b, and 10c), there is a notable drop in the region between the layers due to the obstacle size, resulting in increased pressure and reduced fluid acceleration in this area. However, the general trend remains consistent across the three indicated Richardson numbers. However, the case in Fig 10b showed higher Nusselt number values, which means that in the case of mixed convection, convective heat transfer dominates more than in cases of forced (Fig. 10a) or natural (Fig. 10c) convection.

Figures 10d, 10e, and 10f represent the first layer porosity of 29% and the second layer porosity of 41%, and Figs. 10g, 10h, and 10i correspond to the first layer porosity of 29% and the

second layer porosity of 66%. In the cases of e, f, g, h, and i, the first value of the Nusselt number is less than 1, and the conduction dominance is noticed. Nusselt number at x-position was the highest in the region between layers Nu_x ~ 110 (Fig. 10d, 10e and 10f) and Nu_x ~ 93 (Fig. 10g, 10h and 10i); hence, as the water has more space to penetrate accessible voids, the fluid transport is favored, and it leads to higher heat transfer.

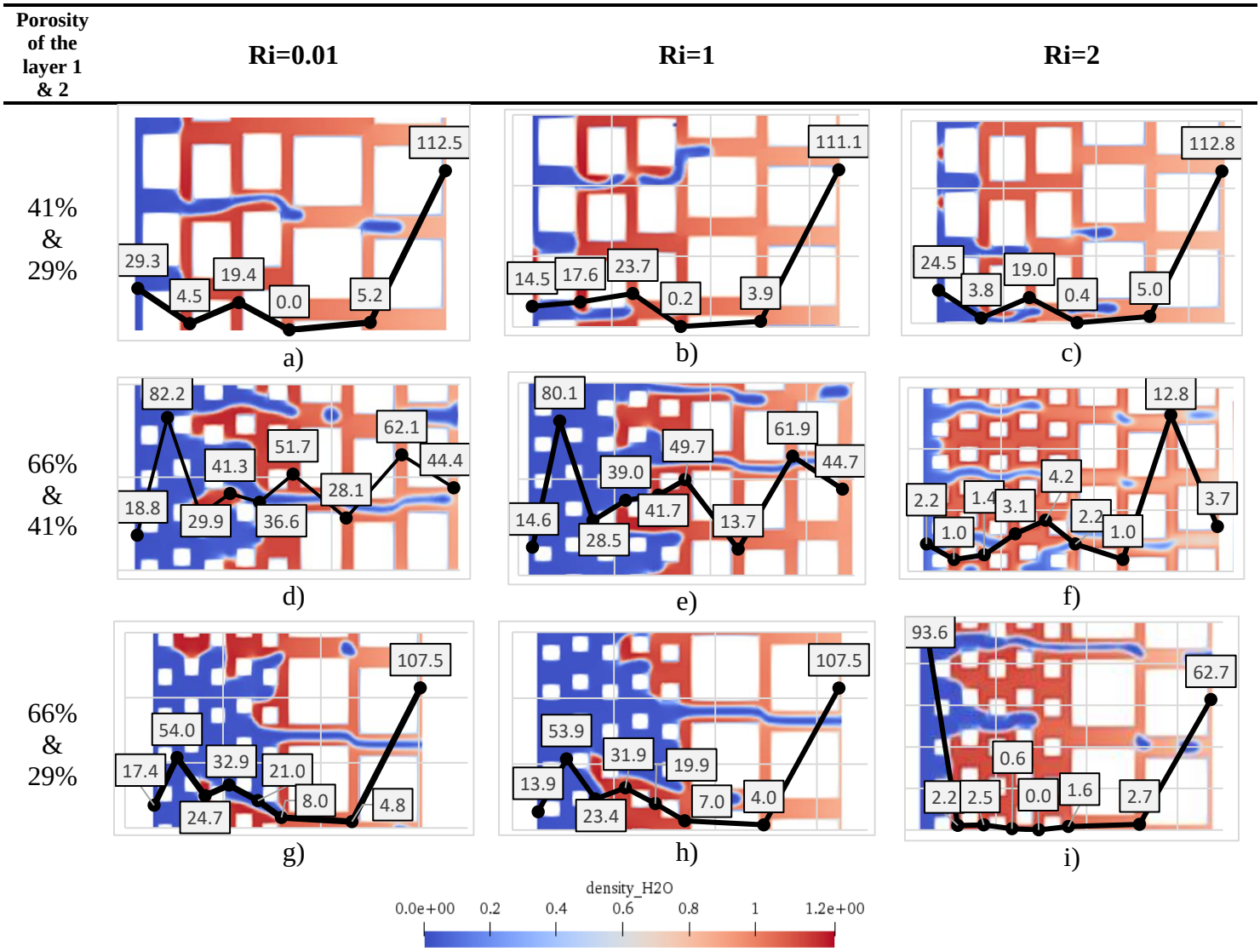

Figure 11. Nusselt number at x-position in the cases of decreasing porosity

Figure 11 illustrates scenarios involving different porosity levels in two layers. When the first layer has a higher porosity and the second layer has a lower porosity, such as in cases (41% & 29%) and (66% & 29%), the dynamics of Nusselt numbers at an x-location remain identical. Notably, the Nusselt number at x is higher in the first layer than in the second. The values at the

end of the second layer are notably high: approximately Nu_x ~ 110 (Fig. 11a, 11b, and 11c), Nu_x ~ 107 (Fig. 11g and 11h), and Nu_x ~ 62.7 (Fig. 11i). This is attributed to the acceleration of the fluid motion and the absence of flow restrictions.

In Figs. 11a, 11b, and 11c, similar Nusselt number values are observed across three Richardson number cases. In the region between the two layers, the Nusselt number is almost 0, indicating the absence of convective heat transfer due to limited fluid movement caused by fewer void spaces. A similar trend is seen in the cases of (66% & 29%), where the Nusselt number at x ranges between 1 and 8. However, in the case of Ri=2 (Fig. 11i), decreasing porosity impacts the development of convective and conductive heat transfer in the scenario of natural convection.

Figures 11d, 11e, and 11f depict the case of a first-layer porosity of 66% and a second-layer porosity of 41%. The dynamics of the Nusselt number at x-location are consistent for forced and mixed convection. In the region between the layers, Nusselt numbers are 51.7 and 49.7 for Ri=0.01 and Ri=1, respectively. The increase in Nusselt numbers in cases of decreasing porosity can be attributed to the enhancement of thermal conductivity and the improvement of heat transfer. The shape of obstacles significantly influences heat transfer. In the scenario where natural convection dominates (Fig. 11f), the Nusselt number is relatively low for the same porosity combination.

6.2. Average Nusselt number

Figures 12, 13, and 14 show the scenarios with increasing porosity of the porous medium.

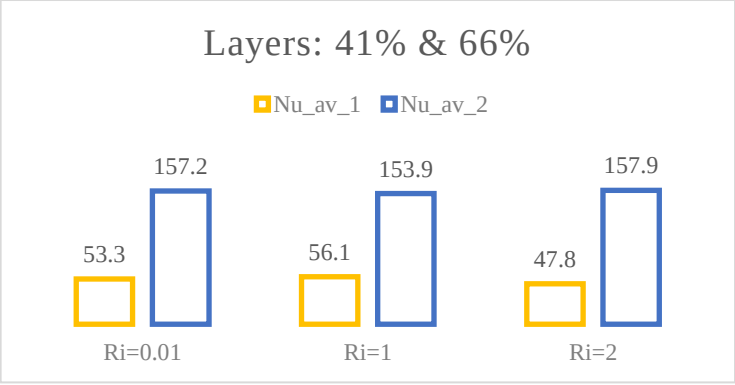

Figure 12. Average Nusselt number for layers with 41% and 66% porosities.

Figure 12 shows the average Nusselt number per layer for the first layer porosity of 41% and the second layer porosity of 66%. In the layer porosity of 41%, the highest Nusselt number is 56.1 in the mixed convection case, which means the mixed convection leads to higher convective

heat transfer. The average Nusselt number in the second layer is almost the same (average value is 156.3) in the three convection cases. The increase in average Nusselt numbers is 99.4, 97.8, and 110.1 for forced, mixed, and natural convection, respectively. The higher convective heat transfer occurred in the case of natural convection in the increasing porosity case (41% & 66%). This phenomenon is due to higher void spaces in the second layer and, consequently, higher fluid movement.

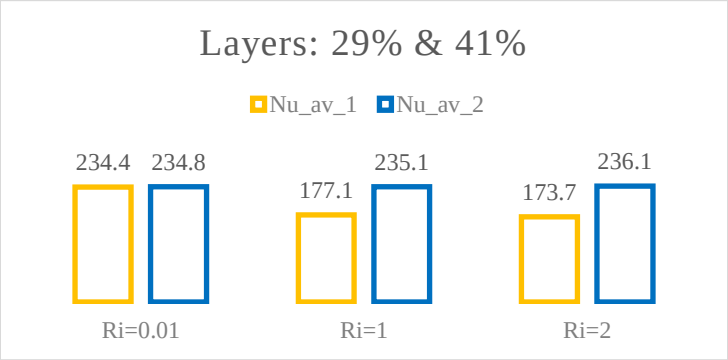

Figure 13. Average Nusselt number for layers with 29% and 41% porosities.

Figure 13 illustrates the average Nusselt number per layer, considering a first-layer porosity of 29% and a second-layer porosity of 41%. For the 29% porosity layer, the highest Nusselt number is 234.5 under forced convection conditions, while the average Nusselt number remains consistent in the second layer. The average Nusselt number exhibits a similar increasing trend in mixed and natural convection scenarios with approximately equal values. The average Nusselt numbers experience an increase of 58 and 62.4 for mixed and natural convection, respectively. Natural convection results in higher convective heat transfer in the case of increasing porosity (29% & 41%). This phenomenon is attributed to the more significant presence of void spaces in the second layer, leading to heightened fluid motion.

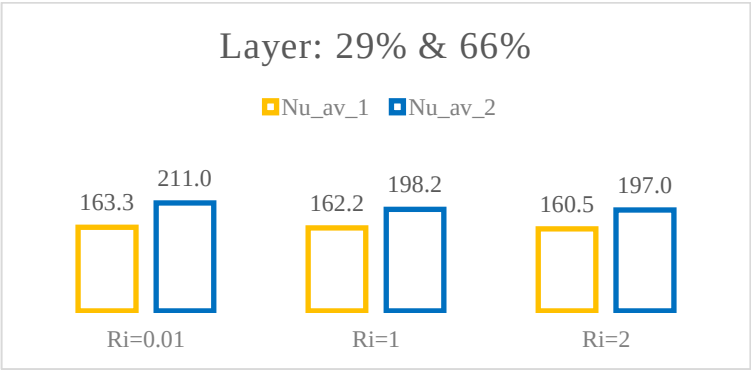

Figure 14. Average Nusselt number for layers with 29% and 66% porosities.

Figure 14 illustrates the average Nusselt number per layer for a first-layer porosity of 29% and a second-layer porosity of 66%. Overall, the trend of the average Nusselt number is consistent across the three cases of convection. In the 29% porosity layer, the highest Nusselt number is 163.3 in the forced convection case, which suggests that forced convection leads to greater convective heat transfer. Similarly, in the 66% porosity layer, the highest Nusselt number is 211 in the forced convection case, further confirming that forced convection results in higher convective heat transfer. The increase in average Nusselt numbers is 47.7, 36, and 37 for forced, mixed, and natural convection, respectively. Notably, higher convective heat transfer is observed in the case of forced convection in the scenario of increasing porosity (29% & 66%). This phenomenon is attributed to higher void spaces in the second layer, increasing fluid movement.

Figures 15, 16, and 17 show the scenarios with decreasing porosity of the porous medium.

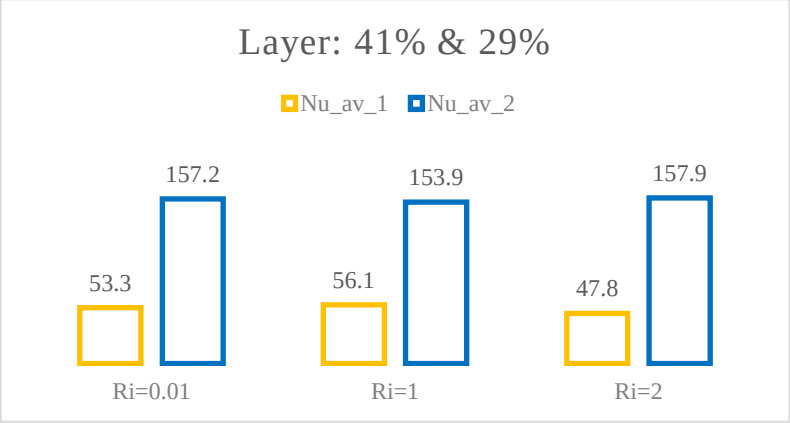

Figure 15. Average Nusselt number for layers with 41% and 29% porosities.

Figure 15 illustrates the average Nusselt number per layer for a first-layer porosity of 41% and a second-layer porosity of 29%. Average Nusselt number values are consistent across the three cases, with the average value in the first layer being 52.4 and in the second layer being 154.8. The increase in the Average Nusselt number is 103.9, 97.8, and 110.1 for Richardson numbers of 0.01, 1, and 2, respectively. The most significant increase in convective heat transfer occurred in the case of free convection. It was observed that decreasing porosity leads to a higher mean temperature of the outlet flow, indicating an increase in heat transfer [45].

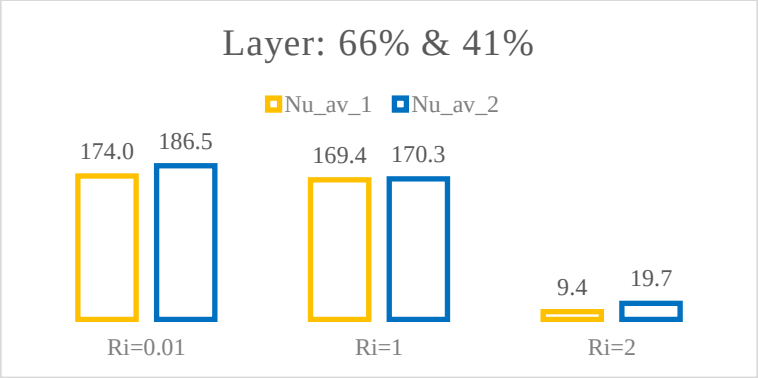

Figure 16. Average Nusselt number for layers with 66% and 41% porosities.

Figure 16 depicts the average Nusselt number per layer for a first-layer porosity of 41% and a second-layer porosity of 29%. Across the three cases of convection, there is a slight increase in the values for both layers. Specifically, for forced convection, the difference is 12.5; for mixed convection, it is 0.9; and for natural convection, it is 10.3. Notably, in the case of natural convection (Ri=2), heat transfer is not significantly convective because the fluid flow was heavily obstructed, preventing the full development of heat transfer in free convection.

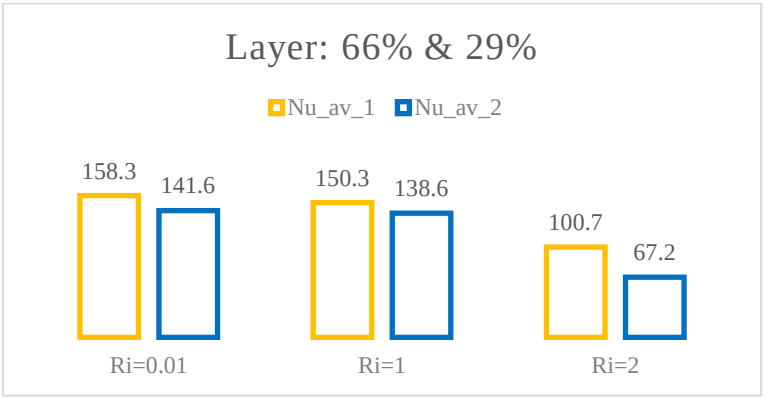

Figure 17. Average Nusselt number for layers 66% and 29%.

Figure 17 illustrates the average Nusselt number per layer for a first-layer porosity of 66% and a second-layer porosity of 29%. Across the three cases of convection, there is a slight decrease in the values for both layers. Specifically, for forced convection, the difference is 16.7; for mixed convection, it is 11.7; and for natural convection, it is 33.5. Significantly, the values in free convection are lower, similar to those observed in Fig. 16. However, the decrease in flow momentum due to large obstacles (29% porosity) restricts fluid flow acceleration, reducing heat conductivity and heat transfer.

6.3. Water displacement

Figure 18 shows water (blue fluid) displacement by CO_2 (red fluid, density_0).

Porosity of the layer 1 & 2	Ri=0.01	Ri=1	Ri=2
29% & 41%	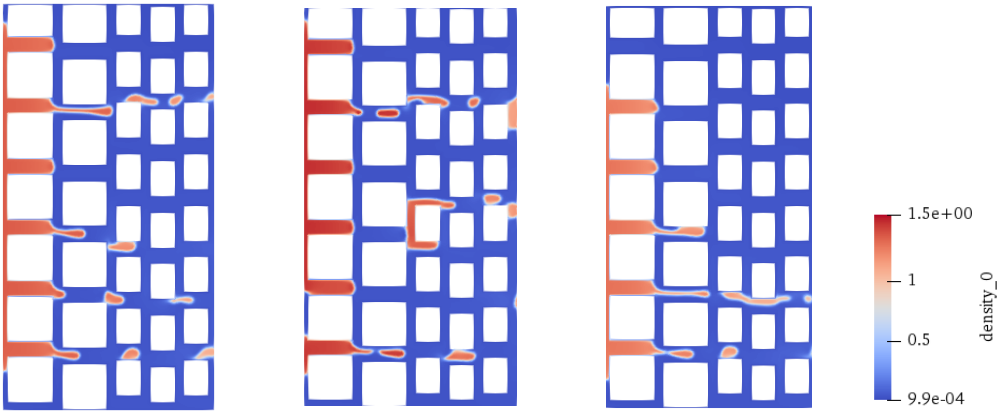		
29% & 66%	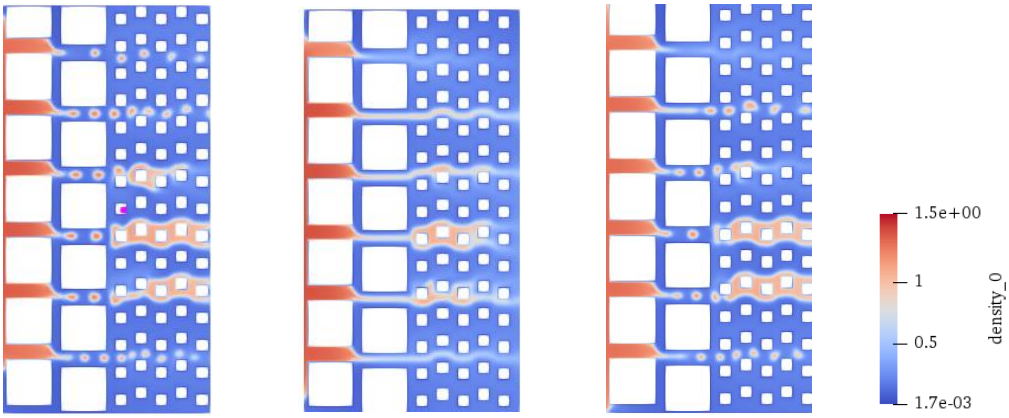		
41% & 66%	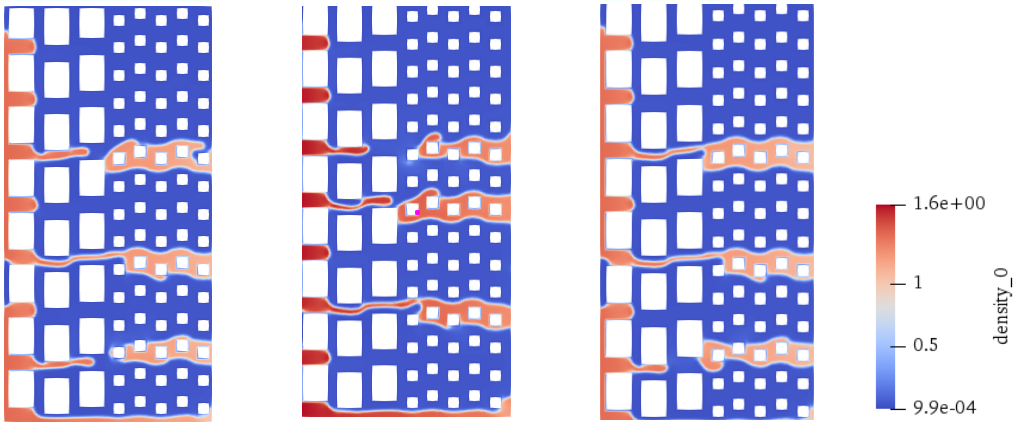		

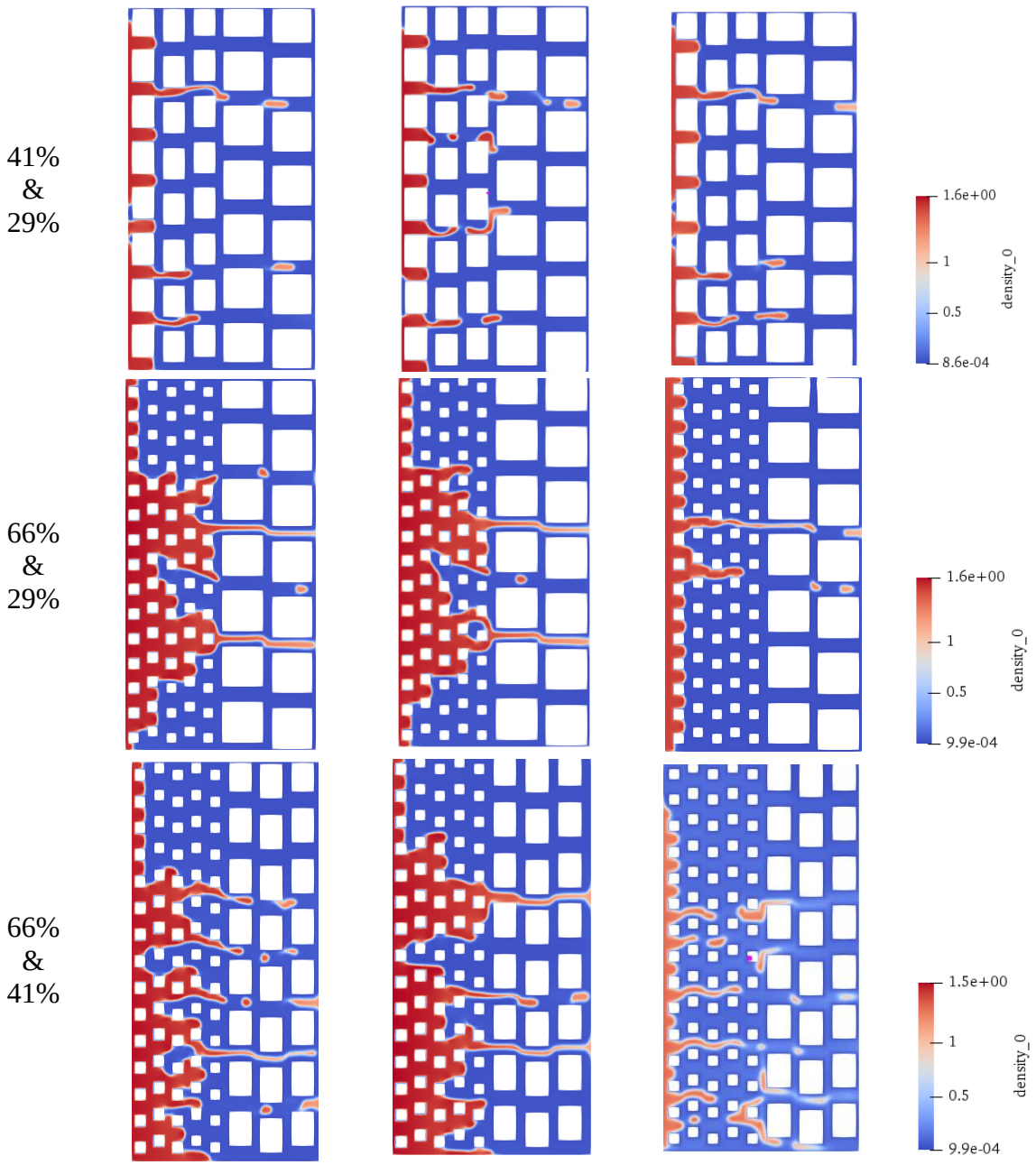

Figure 18. Water displacement by CO_2 in 55000 ts

Figure 18 shows the droplet production of CO_2 and water. These droplets are referred to as an emulsion composed of water and CO_2. This behavior is associated with channel size, which is at the nanoscale. Despite its immiscible nature, the model may identify modest miscible fluid behavior as the pressure rises. As the contact angle of CO_2 in water-saturated media increases and the density of CO_2 increases, CO_2 adhered to the surface progressively detaches from the obstacle walls and forms droplets [53]. Furthermore, the numerical model revealed a channel outlet induced

by the flow-focusing mechanism, which appears to be impacted by the slip velocity between the two fluids [54].

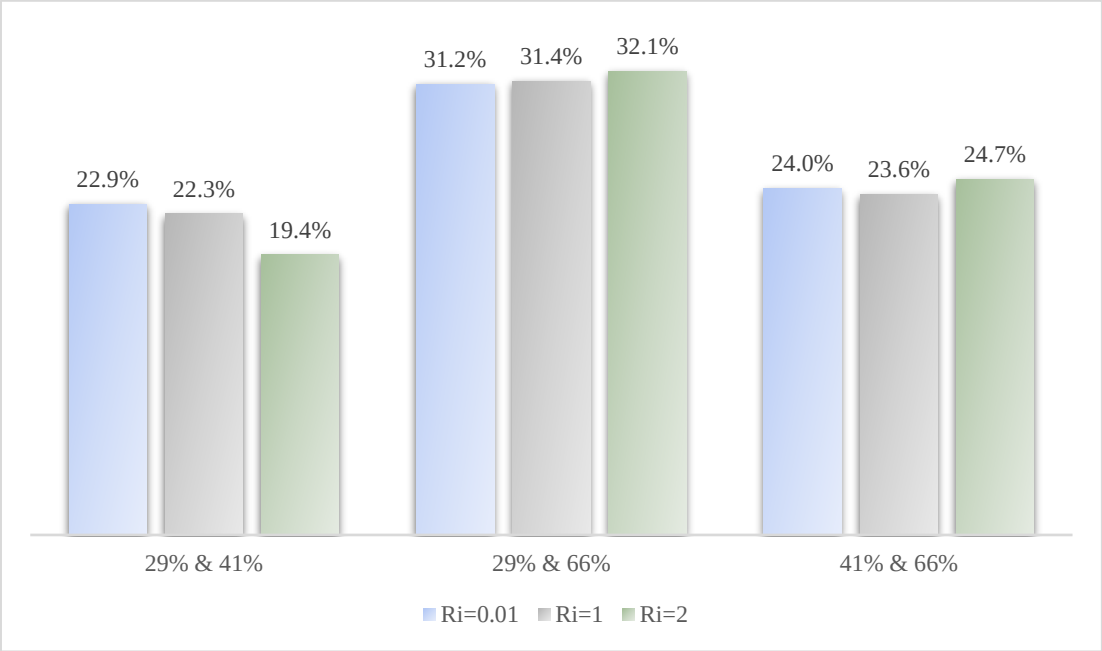

Figure 19. Water fraction displaced in the increasing porosity cases.

Figure 19 illustrates water displacement by CO_2 within a specified time step. The most significant displacement occurred in layers with porosities of 29% and 66%, resulting in the displacement of 30% of the water. This highest displacement was observed under natural convection conditions in the increasing layers' porosity. The amount of water replaced in the layers with porosities of 41% and 66% and 29% and 41% is the same.

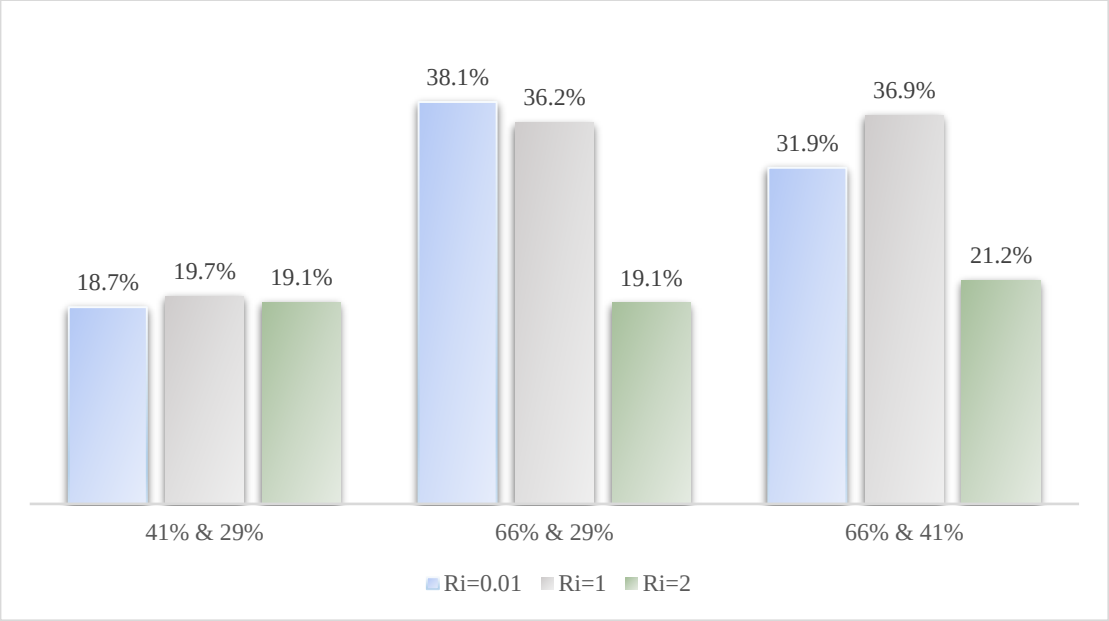

Figure 20. Water fraction displaced in the decreasing porosity cases.

Figure 20 depicts the displacement of water by CO_2 with decreasing porosity of layers. In the case of 41% & 29% porosity layers, the fraction of water displaced is the lowest, averaging 19.1%. The lowest displacement occurred within the decreasing porosity layers in the natural convection scenario. The highest displacement of water, reaching 38.1%, is observed in the 66% & 29% porosity layers under forced convection conditions. Additionally, the highest displacements in mixed convection are noted for the cases of 66% & 29% and 66% & 41% porosity layers.

Chapter 7 – Conclusion

This work used the mesoscopic Lattice Boltzmann Method (LBM) with parallel computing to analyze fluid displacement and heat transfer during CO_2 injection into vertical porous layers of various porosities initially saturated with water and sandwiched between parallel heating plates. Six combinations of porous layers were applied to study the effect of porous medium on CO_2 transport and heat transfer. Additionally, parallel computing was used in the simulation.

The analysis of the effect of porous layers on heat transfer determined that with increasing porosity, heat transfer will also increase, and heat transfer gradually increases in the cases of natural convection. However, in the case of decreasing porosity of layers, convective heat transfer rises significantly four times higher than in the case of increasing porosity. In the case of decreasing porosity for 66% and 29%, there was a slight decrease in the average Nusselt number. The results section shows that heat transfer increases with higher Richardson numbers and decreases in the forced and mixed convection cases. Noticeably, heat transfer is greatly affected by the obstacle size; the larger the obstacle, the more heat transfer is inversely proportional.

The highest water displacement was observed in the cases 66% and 29% porosities with forced convection (Ri=0.01) due to the higher void spaces in the first layer, which made CO_2 flow more easily. Overall, water displacement was higher in the forced convection with increasing porosity and mixed convection with decreasing porosity.

During the water displacement by CO_2, we observed the emergence of droplets, an emulsion comprising water and CO_2. Despite the model's assumption of immiscibility between the fluids, we noted the potential for modest mixing as pressure increased. As the contact angle of CO_2 in water-rich environments increased alongside its density, CO_2 particles gradually disengaged from the obstacle surfaces, forming droplets. Additionally, our numerical model revealed the constriction of the channel at its outlet due to the flow-focusing mechanism, likely influenced by the relative velocities of the two fluids.

Future research might utilize the Peng-Robinson equation of state (EOS) for stability and complex formulations. This EOS will lead to employing models with higher accuracy and near real-life problems. Additionally, varying density and viscosity applications will lead to better

results and an understanding of the flow behavior in a porous medium. Obstacles can be replaced with impedance terms in the code to improve the model.

References

[1] International Energy Agency, "Global Energy Review: CO2 Emissions in 2021.," 2022.

[2] J. Li, Y. Hou, P. Wang, and B. Yang, "A Review of Carbon Capture and Storage Project Investment and Operational Decision-Making Based on Bibliometrics," *Energies*, vol. 12, no. 1, p. 23, Dec. 2018, doi: https://doi.org/10.3390/en12010023.

[3] T. Laconde, "Carbon capture and sequestration : A solution that is struggling to materialise," Climate Chance Association, 2018. Available: https://www.climate-chance.org/en/card/carbon-capture-sequestration-solution-struggling-materialise/

[4] C.-F. Tsang, S. M. Benson, B. Kobelski, and R. E. Smith, "Scientific considerations related to regulation development for CO2 sequestration in brine formations," *Environmental Geology*, vol. 42, no. 2–3, pp. 275–281, Mar. 2002, doi: https://doi.org/10.1007/s00254-001-0497-4.

[5] H. Huang, J.-J. Huang, and X.-Y. Lu, "Study of immiscible displacements in porous media using a color-gradient-based multiphase lattice Boltzmann method," *Computers & Fluids*, vol. 93, pp. 164–172, Apr. 2014, doi: https://doi.org/10.1016/j.compfluid.2014.01.025.

[6] Timm Krüger *et al.*, *Lattice Boltzmann Method Principles and Practice*. Cham Springer International Publishing Springer, 2018.

[7] J. Derksen, D. Eskin, L.-S. Luo, and M. Krafczyk, "Mesoscopic methods in engineering and science," *Computers & Mathematics with Applications*, vol. 65, no. 2, pp. 127–128, Jan. 2013, doi: https://doi.org/10.1016/j.camwa.2012.12.010.

[8] S. Lu, J. Zhu, D. Gao, W. Chen, and X. Li, "Lattice Boltzmann simulation for natural convection of supercritical CO_2 in an inclined square cavity," *International Journal of Numerical Methods for Heat & Fluid Flow*, vol. 30, no. 7, pp. 3635–3652, Nov. 2019, doi: https://doi.org/10.1108/hff-08-2019-0641.

[9] Y.-L. He, Q. Liu, Q. Li, and W.-Q. Tao, "Lattice Boltzmann methods for single-phase and solid-liquid phase-change heat transfer in porous media: A review," *International Journal of Heat and Mass Transfer*, vol. 129, pp. 160–197, Feb. 2019, doi: https://doi.org/10.1016/j.ijheatmasstransfer.2018.08.135.

[10] M. J. Blunt, *Multiphase Flow in Permeable Media*. London: Cambridge University Press, 2017. doi: https://doi.org/10.1017/9781316145098.

[11] C. SHU, Y. PENG, and Y. T. CHEW, "Simulation Of Natural Convection In A Square Cavity By Taylor Series Expansion- And Least Squares-Based Lattice Boltzmann Method," *International Journal of Modern Physics C*, vol. 13, no. 10, pp. 1399–1414, Dec. 2002, doi: https://doi.org/10.1142/s0129183102003966.

[12] A. D'Orazio, M. Corcione, and G. P. Celata, "Application to natural convection enclosed flows of a lattice Boltzmann BGK model coupled with a general purpose thermal boundary

condition," *International Journal of Thermal Sciences*, vol. 43, no. 6, pp. 575–586, Jun. 2004, doi: https://doi.org/10.1016/j.ijthermalsci.2003.11.002.

[13] Z. Guo and T. S. Zhao, "Lattice Boltzmann simulation of natural convection with temperature-dependent viscosity in a porous cavity," *Progress in Computational Fluid Dynamics, An International Journal*, vol. 5, no. 1/2, p. 110, 2005, doi: https://doi.org/10.1504/pcfd.2005.005823.

[14] W.-W. YAN, Y. LIU, Z.-L. GUO, and Y.-S. XU, "Lattice Boltzmann Simulation On Natural Convection Heat Transfer In A Two-Dimensional Cavity Filled With Heterogeneously Porous Medium," *International Journal of Modern Physics C*, vol. 17, no. 06, pp. 771–783, Jun. 2006, doi: https://doi.org/10.1142/s0129183106009291.

[15] C. Y. Zhao, L. N. Dai, G. H. Tang, Z. G. Qu, and Z. Y. Li, "Numerical study of natural convection in porous media (metals) using Lattice Boltzmann Method (LBM)," *International Journal of Heat and Fluid Flow*, vol. 31, no. 5, pp. 925–934, Oct. 2010, doi: https://doi.org/10.1016/j.ijheatfluidflow.2010.06.001.

[16] H. M. Ouakad, "Modeling the CO2 Sequestration Convection Problem Using the Lattice Boltzmann Method," *Mathematical Problems in Engineering*, vol. 2013, pp. 1–10, 2013, doi: https://doi.org/10.1155/2013/846854.

[17] Jian.-F. . Xie, S. He, Y. Q. Zu, B. Lamy-Chappuis, and B. W. D. Yardley, "Relative permeabilities of supercritical CO2 and brine in carbon sequestration by a two-phase lattice Boltzmann method," *Heat and Mass Transfer*, vol. 53, no. 8, pp. 2637–2649, Mar. 2017, doi: https://doi.org/10.1007/s00231-017-2007-6.

[18] X.-B. Feng, Q. Liu, and Y.-L. He, "Numerical simulations of convection heat transfer in porous media using a cascaded lattice Boltzmann method," *International Journal of Heat and Mass Transfer*, vol. 151, p. 119410, Apr. 2020, doi: https://doi.org/10.1016/j.ijheatmasstransfer.2020.119410.

[19] S. Chen, W. Li, and H. I. Mohammed, "Heat transfer of large Prandtl number fluids in porous media by a new lattice Boltzmann model," *International Communications in Heat and Mass Transfer*, vol. 122, p. 105129, Mar. 2021, doi: https://doi.org/10.1016/j.icheatmasstransfer.2021.105129.

[20] E. J. Braga and M. J. S. de Lemos, "Turbulent natural convection in a porous square cavity computed with a macroscopic κ–ε model," *International Journal of Heat and Mass Transfer*, vol. 47, no. 26, pp. 5639–5650, Dec. 2004, doi: https://doi.org/10.1016/j.ijheatmasstransfer.2004.07.017.

[21] Y. Cao, "Variable property-based lattice Boltzmann flux solver for thermal flows in the low Mach number limit," *International Journal of Heat and Mass Transfer*, vol. 103, pp. 254–264, Dec. 2016, doi: https://doi.org/10.1016/j.ijheatmasstransfer.2016.07.052.

[22] Q. Liu and Y.-L. He, "Lattice Boltzmann simulations of convection heat transfer in porous media," *Physica A: Statistical Mechanics and its Applications*, vol. 465, pp. 742–753, Jan. 2017, doi: https://doi.org/10.1016/j.physa.2016.08.010.

[23] P. L. Bhatnagar, E. P. Gross, and M. Krook, "A Model for Collision Processes in Gases. I. Small Amplitude Processes in Charged and Neutral One-Component Systems," *Physical Review*, vol. 94, no. 3, pp. 511–525, May 1954, doi: https://doi.org/10.1103/physrev.94.511.

[24] L. Chen, Q. Kang, Y. Mu, Y.-L. He, and W.-Q. Tao, "A critical review of the pseudopotential multiphase lattice Boltzmann model: Methods and applications," *International Journal of Heat and Mass Transfer*, vol. 76, pp. 210–236, Sep. 2014, doi: https://doi.org/10.1016/j.ijheatmasstransfer.2014.04.032.

[25] Z. Guo and T. S. Zhao, "A Lattice Boltzmann Model For Convection Heat Transfer In Porous Media," *Numerical Heat Transfer, Part B: Fundamentals*, vol. 47, no. 2, pp. 157–177, Jan. 2005, doi: https://doi.org/10.1080/10407790590883405.

[26] D. R. Hewitt, "Vigorous convection in porous media," *Proceedings of The Royal Society A: Mathematical, Physical and Engineering Sciences*, vol. 476, no. 2239, pp. 20200111–20200111, Jul. 2020, doi: https://doi.org/10.1098/rspa.2020.0111.

[27] M. Elenius and S. E. Gasda, "Convective mixing in formations with horizontal barriers," *Advances in Water Resources*, vol. 62, pp. 499–510, Dec. 2013, doi: https://doi.org/10.1016/j.advwatres.2013.10.010.

[28] E. B. Soboleva, "Density-driven convection in an inhomogeneous geothermal reservoir," *International Journal of Heat and Mass Transfer*, vol. 127, pp. 784–798, Dec. 2018, doi: https://doi.org/10.1016/j.ijheatmasstransfer.2018.08.019.

[29] K. S. Bharath, C. K. Sahu, and M. R. Flynn, "Isolated buoyant convection in a two-layered porous medium with an inclined permeability jump," *Journal of Fluid Mechanics*, vol. 902, Sep. 2020, doi: https://doi.org/10.1017/jfm.2020.599.

[30] C. K. Sahu and M. R. Flynn, "The Effect of Sudden Permeability Changes in Porous Media Filling Box Flows," *Transport in Porous Media*, vol. 119, no. 1, pp. 95–118, Jun. 2017, doi: https://doi.org/10.1007/s11242-017-0875-3.

[31] D. R. Hewitt, G. G. Peng, and J. Lister, "Buoyancy-driven plumes in a layered porous medium," *Journal of Fluid Mechanics*, vol. 883, Nov. 2019, doi: https://doi.org/10.1017/jfm.2019.888.

[32] Ashwanth Salibindla, Rabin Subedi, V. C. Shen, M. Masuk, and R. Ni, "Dissolution-driven convection in a heterogeneous porous medium," *Journal of Fluid Mechanics*, vol. 857, pp. 61–79, Oct. 2018, doi: https://doi.org/10.1017/jfm.2018.732.

[33] D. R. Hewitt, "Evolution of convection in a layered porous medium," *Journal of Fluid Mechanics*, vol. 941, May 2022, doi: https://doi.org/10.1017/jfm.2022.335.

[34] B. He, S. Lu, D. Gao, W. Chen, and F. Lin, "Lattice Boltzmann simulation of double diffusive natural convection in heterogeneously porous media of a fluid with temperature-dependent viscosity," *Chinese Journal of Physics*, vol. 63, pp. 186–200, Feb. 2020, doi: https://doi.org/10.1016/j.cjph.2019.10.027.

[35] K.-Q. Xia, "Current trends and future directions in turbulent thermal convection," *Theoretical and Applied Mechanics Letters*, vol. 3, no. 5, p. 052001, 2013, doi: https://doi.org/10.1063/2.1305201.

[36] F. Bahadori, F. Rashidi, F. Bahadori, and F. Rashidi, "Analytical Solution of Thermo-Diffusion and Diffusion-Thermo Effects on Heat and Mass Transfer in a Composite Porous Media," *Contemporary Engineering Sciences*, vol. 5, no. 2, pp. 59–65, 2012.

[37] S. C. Mishra, S. Panigrahy, and V. J. Ghatage, "Analysis of combined mode heat transfer in a porous medium using the lattice Boltzmann method," *Numerical Heat Transfer, Part A: Applications*, vol. 69, no. 10, pp. 1092–1105, Mar. 2016, doi: https://doi.org/10.1080/10407782.2015.1125711.

[38] V. K. Mishra, S. C. Mishra, and D. N. Basu, "Simultaneous Estimation of Properties in a Combined Mode Conduction-Radiation Heat Transfer in a Porous Medium," *Heat Transfer-Asian Research*, vol. 45, no. 8, pp. 699–713, Jun. 2015, doi: https://doi.org/10.1002/htj.21184.

[39] A. Ashirbekov, B. Kabdenova, E. Monaco, and L. R. Rojas-Solórzano, "Equation of State's Crossover Enhancement of Pseudopotential Lattice Boltzmann Modeling of CO2 Flow in Homogeneous Porous Media," *Fluids*, vol. 6, no. 12, p. 434, Dec. 2021, doi: https://doi.org/10.3390/fluids6120434.

[40] Takaji Inamuro, M. Yoshino, H. Inoue, R. Mizuno, and F. Ogino, "A Lattice Boltzmann Method for a Binary Miscible Fluid Mixture and Its Application to a Heat-Transfer Problem," *Journal of Computational Physics*, vol. 179, no. 1, pp. 201–215, Jun. 2002, doi: https://doi.org/10.1006/jcph.2002.7051.

[41] M. Yoshino and Takaji Inamuro, "Lattice Boltzmann simulations for flow and heat/mass transfer problems in a three-dimensional porous structure," *International Journal for Numerical Methods in Fluids*, vol. 43, no. 2, pp. 183–198, Aug. 2003, doi: https://doi.org/10.1002/fld.607.

[42] Z. Guo, B. Shi, and C. Zheng, "A coupled lattice BGK model for the Boussinesq equations," *International Journal for Numerical Methods in Fluids*, vol. 39, no. 4, pp. 325–342, Jan. 2002, doi: https://doi.org/10.1002/fld.337.

[43] F. Fornarelli, A. Lippolis, and Paolo Oresta, "Buoyancy Effect on the Flow Pattern and the Thermal Performance of an Array of Circular Cylinders," *Journal of heat transfer*, vol. 139, no. 2, Oct. 2016, doi: https://doi.org/10.1115/1.4034794.

[44] T. L. Bergman and E. Al, Fundamentals of heat and mass transfer, 7th ed. Hoboken: J. Wiley & Sons, Cop, 2011.

[45] A. Abouei Mehrizi, M. Farhadi, K. Sedighi, and M. Aghajani Delavar, "Effect of fin position and porosity on heat transfer improvement in a plate porous media heat exchanger," Journal of the Taiwan Institute of Chemical Engineers, vol. 44, no. 3, pp. 420–431, May 2013, doi: https://doi.org/10.1016/j.jtice.2012.12.018.

[46] B. E. Rapp, *Microfluidics : Modeling, Mechanics, and Mathematics*. Amsterdam Elsevier, 2017, pp. 257–259.
[47] L. Wang *et al.*, "Review of multi-scale and multi-physical simulation technologies for shale and tight gas reservoirs," *Journal of Natural Gas Science and Engineering*, vol. 37, pp. 560–578, Jan. 2017, doi: https://doi.org/10.1016/j.jngse.2016.11.051.

[47] L. Wang *et al.*, "Review of multi-scale and multi-physical simulation technologies for shale and tight gas reservoirs," *Journal of Natural Gas Science and Engineering*, vol. 37, pp. 560–578, Jan. 2017, doi: https://doi.org/10.1016/j.jngse.2016.11.051.

[48] R. M. Clever and F. H. Busse, "Transition to time-dependent convection," *Journal of Fluid Mechanics*, vol. 65, no. 4, pp. 625–645, Oct. 1974, doi: https://doi.org/10.1017/s0022112074001571.

[49] N. I. Prasianakis and I. V. Karlin, "Lattice Boltzmann method for simulation of compressible flows on standard lattices," *Physical Review E*, vol. 78, no. 1, Jul. 2008, doi: https://doi.org/10.1103/physreve.78.016704.

[50] Armin Haghshenas and Mohammad Hassan Rahimian, "Simulation of Two-Phase Rayleigh-Benard Problem Using Lattice Boltzmann Method," *International advanced research journal in science, engineering and technology*, vol. 2, no. 10, pp. 1–6, Oct. 2015, doi: https://doi.org/10.17148/iarjset.2015.21001.

[51] Y. Verma, V. Vishal, and P. G. Ranjith, "Sensitivity Analysis of Geomechanical Constraints in CO2 Storage to Screen Potential Sites in Deep Saline Aquifers," *Frontiers in Climate*, vol. 3, Oct. 2021, doi: https://doi.org/10.3389/fclim.2021.720959.

[52] K. Michael *et al.*, "Geological storage of CO2 in saline aquifers—A review of the experience from existing storage operations," *International Journal of Greenhouse Gas Control*, vol. 4, no. 4, pp. 659–667, Jul. 2010, doi: https://doi.org/10.1016/j.ijggc.2009.12.011.

[53] H. Wang *et al.*, "Pore-Scale Study on Shale Oil–CO_2–Water Miscibility, Competitive Adsorption, and Multiphase Flow Behaviors," *Langmuir*, vol. 39, no. 34, pp. 12226–12234, Aug. 2023, doi: https://doi.org/10.1021/acs.langmuir.3c01570.

[54] K. Granado, S. Anna, L. Rojas-Solórzano, and S. Verma, "Numerical simulation of droplet formation in a microchannel device," *The International Journal of Multiphysics*, vol. 7, no. 4, pp. 271–286, Dec. 2013, doi: https://doi.org/10.1260/1750-9548.7.4.271.

Appendix A: Parallel Computing

This chapter will discuss parallel computing. This thesis used Parallel computing to improve the DL-MESO open-source software performance. Previous theses developed by our research team used the sequential or serial version of the software's solver computing capacity. Parallel computing was used in this project with the Ubuntu operating system (Fig. 21). Ten cores out of 16 were used to speed up the simulation without damaging the system.

```
% Initial prompt as root user
suroot@000297755NU:~# su little
% Switched to user 'little', prompt changes accordingly
little@000297755NU:/root$ cd ..
% Changed directory to parent directory
little@000297755NU:/$ cd mnt/c/Users/nurbakyt.marat/Desktop/two\ layers/Ri\=0/29\ 41/
% Changed directory to the specified path, note the use of escape characters for spaces and special characters
little@000297755NU:/mnt/c/Users/nurbakyt.marat/Desktop/two layers/Ri=0/29 41$ mpirun -np 10 plbe
% Ran the command 'mpirun' with 10 processes (-np 10) executing the 'plbe' program
\end{lstlisting}
```

Fig.21 Ubuntu Prompt for parallel computing.

Table 4 shows the cases of 29% and 41%, and Richardson numbers are 0 and 1. Table 4 demonstrates that with parallel computing, simulation ended 11 times earlier. Parallelism helped make simulations faster, as conventional solver computing takes more than 5 hours, while parallel computing ended in half an hour.

Table 4: Parallel and Serial computing comparisons using the DL_MESO in benchmark case:

Cases	Serial computing (seconds)	Parallel computing (seconds)
Ri=0, 29% & 41% porosity	19046	1608
Ri=1, 29% & 41% porosity	15412	1352

Appendix B: Code for obstacles with adiabatic BC

Matlab code for adiabatic boundary conditions of obstacles is used in SPA file as input.

```
a = [250 50]; % Co-ordinate of 1st Point
b = [300 100]; % Co-ordinate of 2nd Point

% Determine Length of Matrix
L1 = b(:,1)-a(:,1)+1;
L2 = b(:,end)-a(:,end)+1;
A = zeros(L1*L2,4);

A(:,4) = 12; % Give all Points Value/constrain 11 in the start

% Determine Co-ordinates of all Points
c=1;
f = a(:,2);
for j=1:L2
   d = c;
   e = a(:,1);
   for i=1:L1
     A(d,1:2) = [e f];
     d = d+1;
     e = e+1;
   end
   c = d;
   f = f+1;
end

% Boundary Values/Constrains
for i=1:L1
   A(i,4) = 249;
end
for i=length(A):-1:length(A)-L1+1
   A(i,4) = 247;
end
for i =1:L1:length(A)-L1+1
  A(i,4) = 248;
  A(i+L1-1,4) = 250;
end
% Edges Values/Conttrains
A(1,4) = 233;
A(L1,4) = 234;
A(end-L1+1,4) = 232;
A(end,4) = 231;
writematrix(A,'obstacle.txt','Delimiter','space')
```